3D Wire Mesh Photonic Crystals

D. F. Sievenpiper, M. E. Sickmiller, and E. Yablonovitch
Electrical Engineering Department, University of California, Los Angeles, California 90095-1594
(Received 30 October 1995)

We have investigated the electromagnetic properties of a 3D wire mesh in a geometry resembling covalently bonded diamond. The frequency and wave vector dispersion show forbidden bands at those frequencies ν_0, corresponding to the lattice spacing, just as dielectric photonic crystals do. But they have a new forbidden band which commences at zero frequency and extends, in our geometry, to $\sim\frac{1}{2}\nu_0$, acting as a type of plasma cutoff frequency. Wire mesh photonic crystals appear to support a longitudinal plane wave, as well as two transverse plane waves. We identify an important new regime for microwave photonic crystals, an effective medium limit, in which electromagnetic waves penetrate deeply into the wire mesh through the aid of an impurity band.

PACS numbers: 42.25.Bs, 41.20.Jb, 78.90.+t, 84.40.–x

In the past few years the concepts of solid state physics have been brought to bear on [1] electromagnetism and Maxwell's equations. Artificial three-dimensional dielectric structures have been observed [2–5], which are the photonic analog of a semiconductor [6,7]. In these "photonic crystals" a photonic band gap arises in which electromagnetic modes, spontaneous emission, and zero-point fluctuations are all absent. A dielectric photonic crystal containing a local defect forms an optical 3D microcavity [8]. Since metals are usually quite lossy at optical frequencies, most photonic crystal work has focused on dielectric structures. Nevertheless, metallic 3D structures can be valuable at microwave frequencies. Two-dimensional metallic structures are already being investigated [9] and theoretical work has recently begun [10–12] on 3D metallic photonic crystals. We will show in this paper that 3D wire mesh electromagnetic structures have very different physics from the dielectric photonic crystals which were studied previously.

In choosing a particular 3D wire mesh geometry we were influenced by an extension of the intuitively natural two-dimensional hexagonal wire mesh geometry, into the third dimension. The electronic material analog of a hexagonal wire mesh is graphite structure, and the corresponding extension into three dimensions is diamond structure. Indeed, it has already been shown for 3D dielectric photonic crystals that the diamond geometry [2] has an unusually intimate link with Maxwell's equations. Therefore the wire mesh structure we have chosen consists of a diamond lattice, in which the "atoms" are geometrical points in space, and the valence bonds connecting those points are copper wires, 1 cm long. The crystal has a $\langle 001 \rangle$ face orientation, and was $11a/\sqrt{2} \times 11a/\sqrt{2}$ wide and $3a$ thick (18 cm $\times$ 18 cm $\times$ 7 cm), where a is the length of the unit cube of our diamond lattice. A photograph of a thin section of our wire mesh structure is shown in Fig. 1. Together with a detailed view of the copper wire strips which snap together to make diamond geometry.

Band structure measurements were performed using a Hewlett-Packard 8720 Network Analyzer, and monopole antennas for transmitting and receiving. The crystal was placed in the window of an anechoic chamber at a range of 1.25 m from the transmitting antenna in order to approximate plane-wave illumination. Our experiments consisted of microwave transmission measurements through the 3D wire mesh structure, as a function of incidence angle and frequency. As expected, narrow forbidden gaps are observed centered at frequencies ν_0, corresponding to the spatial periodicity of the wires. Nonetheless, the most dominant electromagnetic feature of these wire mesh structures is not related to spatial periodicity, but happens to be a deep, sharp, and wide three-dimensional stop band that extends from zero frequency up to a finite frequency ν_p. We observe in our geometry that ν_p is approximately one-half of ν_0. We regard ν_p as being analogous to a type of plasma frequency associated with the motion of electrons in the continuous, interconnected, wire network, constituting our weblike structure. Alternately, it may be considered as a 3D cutoff frequency for wavelengths too large to fit between the rows of wires. A transmission spectrum showing the steep edge at $\nu_p = 6.5$ GHz is displayed in Fig. 3(a). (To the left of the steep edge is a transmission peak produced by a defect mode.)

We attempted to measure the full electromagnetic dispersion in our diamond wire mesh photonic crystal. This required the identification of frequencies and wave vectors for allowed modes. Mode frequencies were identified with step function changes in the transmission spectrum of external plane waves through the structure, while the corresponding internal wave vectors were determined by momentum matching at the surface of the photonic crystal. The projection of the external wave vector onto the surface of the photonic crystal fixed the internal $\langle k_x, k_y, 0 \rangle$, while k_z was determined by physical reasoning as follows: For the lowest frequency step function cutoff, ν_p, the z component was set at $k_z = 0$. For higher forbidden

 0031-9007/96/76(14)/2480(4)$10.00

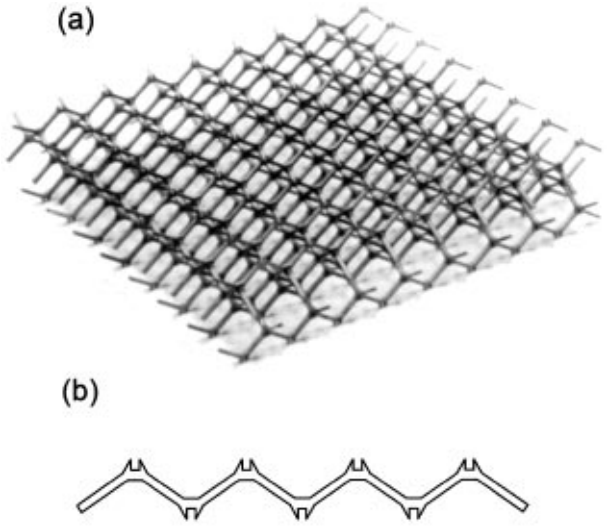

FIG. 1. (a) A perspective photograph of our diamond geometry 3D wire mesh photonic crystal. The individual wires play the role of "valence bonds" connecting the atoms which are merely geometrical points in space. The wires have a 1.25 mm square cross section, and are 1 cm long. (b) A detailed view of the copper wire strips which snap together to make diamond structure.

gaps due to periodicity, k_z was set so that $\vec{k}$ would fall at the surface of the Brillouin zone.

In the wire mesh photonic crystal shown in Fig. 1, the top surface is a $\langle 1, 0, 0\rangle$ cubic plane. Normal incidence puts the wave vector in the *X* direction of reciprocal space, as shown in the Brillouin zone inset of Fig. 2. Repeated spectra were taken as the sample was rotated away from normal incidence, so that the wave vector moved along the *X*-*U*-*L* line. The procedure was repeated along the *X*-*W*-*K* line and for both *s* and *p* polarizations. With the wave vector in the *X*-*W*-*K* direction, its component in the $k_z = 0$ plane, in the vicinity of the Γ point, would be in the Γ-*X* direction (one of the other orthogonal *X* points). Thus an *X*-*W*-*K* scan also covered the Γ-*X* line. Likewise, an *X*-*U*-*L* scan covered the Γ-*K* line in the Γ vicinity, as well. All of the various reciprocal space segments were than stitched together in Fig. 2(a) for *s* polarization and Fig. 2(b) for *p* polarization.

In an experiment such as this, there is no guarantee that every internal mode will be observed. Coupling to certain modes could be forbidden in our geometry, and some internal plane waves might simply couple inefficiently to external plane waves due to mode matching problems at the incident interface. In Fig. 2(a), the modes detected at the *K* point are certainly incomplete, since the *K* point differs by a reciprocal lattice vector from the *U* point, where additional modes are detected. The gap due to periodicity, at the surface of the Brillouin zone, falls between 12 and 13 GHz, but it is not clear that it is an absolute gap in all directions of space. The dominant feature is the low frequency gap from 0 to 6.5 GHz associated with the motion of electrons in the

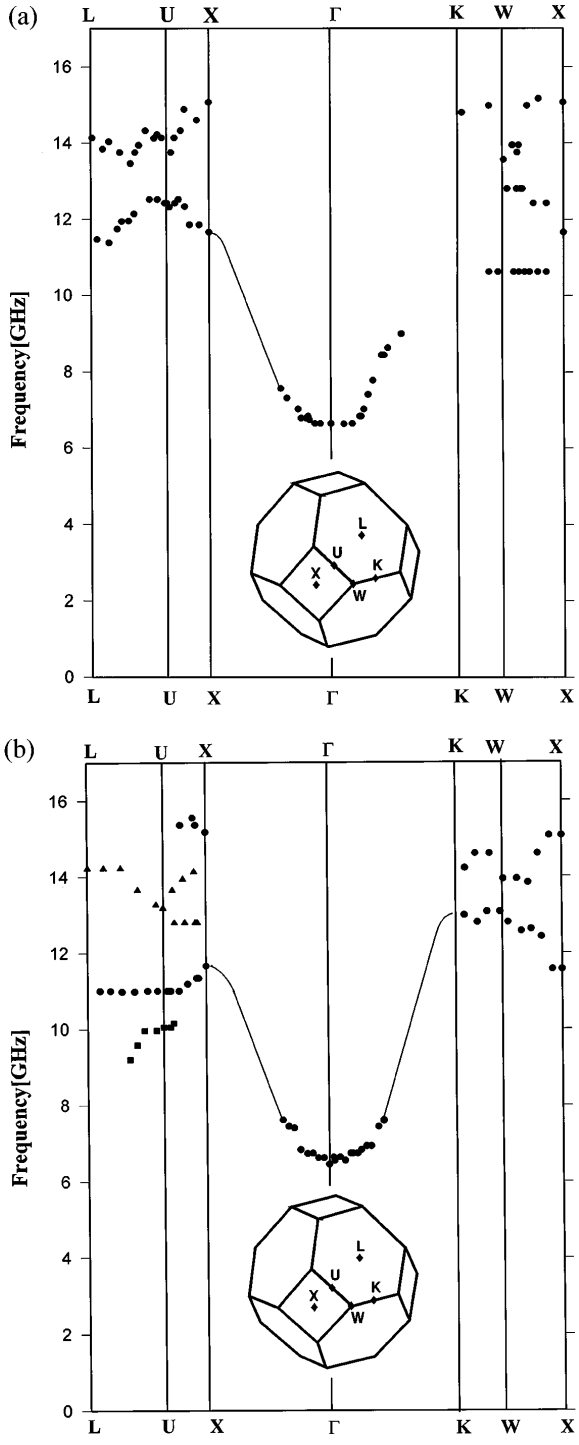

FIG. 2. (a) Frequency and wave vector representing allowed plane waves inside our diamond wire mesh photonic crystal; *s* polarization incident on a $\langle 1, 0, 0\rangle$ face. (b) Dispersion relation for *p* polarization. The triangles represent a mode which vanishes at normal incidence which may be a longitudinal plane wave. The squares may be an experimental artifact.

continuous, interconnected, wire network. For incident *p* polarization, in Fig. 2(b), those modes indicated by triangular dots (along *X*-*U*-*L*) had the property that they

vanished at normal incidence. Therefore these might be internal, longitudinally polarized plane waves similar to surface plasmons, but running along the internal wires of the structure. This implies that wire mesh photonic crystals support a longitudinal plane wave, as well as two transverse plane waves.

Our band structure results for metallic wire mesh photonic crystals may be summarized as follows: (a) Periodicity produces a stop band just as in dielectric photonic crystals (in spite of some speculation that metallic photonic crystals would possess allowed rather than forbidden bands). (b) Wire mesh photonic crystals have a new forbidden band which commences at zero frequency, and extends to approximately half the normal band-gap frequency. (c) Longitudinal modes are allowed in metallic photonic crystals. Therefore the internal electromagnetic plane waves have three possible polarizations, rather than just two.

Let us now discuss the significance of these wire mesh photonic crystal properties. The most interesting point is the plasma edge, or cutoff frequency ν_p. In the vicinity of ν_p the mesh spacing is similar to the vacuum wavelength. Given that microwave lengths are rather large, combined with the need for multiple mesh periods to form a 3D crystal, these considerations would appear to demand inconveniently large structures. It would therefore be preferable to operate the wire mesh photonic crystal at mesh spacing much smaller than a vacuum wavelength. Under those conditions, the electromagnetic radiation generally penetrates only one or two unit cells, effectively interacting with only a two-dimensional surface layer of the wire mesh. Two-dimensional periodic metallic structures are already well known [13–16] in electromagnetic engineering, where they are called "frequency selective surfaces." In order to access a distinctive physical regime, and a potentially useful one, we must design photonic crystal structures where electromagnetic waves penetrate the wire mesh, whose spacing $a \ll \lambda$, the vacuum wavelength. This condition defines a *new and different regime* of photonic crystals.

In the new regime $a \ll \lambda$, the crystal structures are actually effective media, described by a frequency dependent dielectric constant $\varepsilon(\omega)$, rather than the full 3D wave vector dependence $\varepsilon(\vec{k})$ of a true photonic crystal. Nevertheless, such effective media can have many unusual properties, including particularly a negative, predominantly real, dielectric constant at microwave frequencies, which would otherwise be difficult to find among solid metals. Effective medium theory [17–19], as well as its application to cermet [20,21] structures, has been the subject of extensive past study.

Since the local geometry of such an effective medium is probably not as important as it would be in a dielectric photonic crystal, a diamond wire mesh, a cubic [12] wire mesh, or perhaps a random wire mesh may perform similarly. The basic approach toward creating a penetrable medium in which $a \ll \lambda$ is to introduce an impurity band within the low frequency forbidden gap, below ν_p, in other words, a band structure within a band structure, or a superlattice.

In Fig. 3 we present results on the initial stages of a transition from isolated defect modes to impurity band formation, by capacitive defects in the wire mesh, i.e., selectively cut wires. (Independently, Pendry *et al.* [22] have introduced inductive loading of the individual wires to create such a medium.) Measurements of defect resonance were taken with the crystal embedded in microwave absorbing foam. Monopole antenna probes were inserted

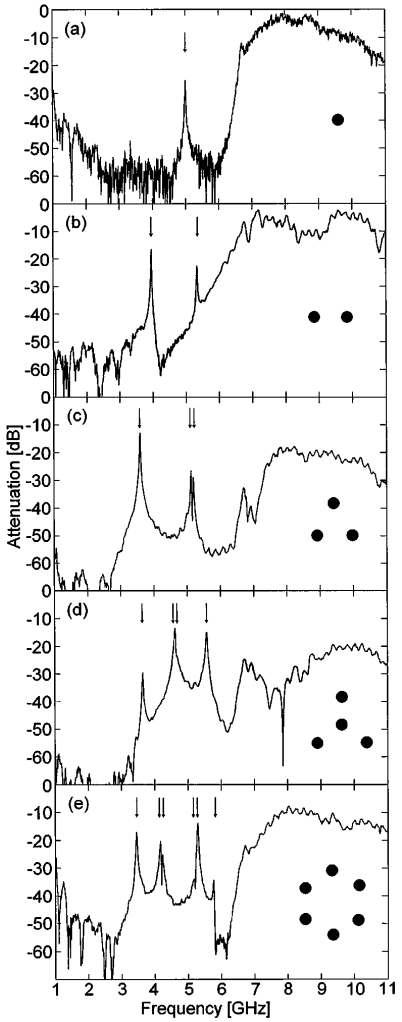

FIG. 3. The evolution from a single defect in the photonic crystal, toward an impurity band within the 0 to 6.5 GHz forbidden gap. The defects were all spatially located within the same $\langle 1, 1, 1 \rangle$ plane. (a) A defect consisting of a single cut wire. (b) Two neighboring cut wires, producing "bonding and antibonding modes" as in a diatomic molecule. (c) Three neighbors resembling a triangular ring molecule. (d) Four in a star configuration. (e) Six in a benzene ring configuration. The vertical arrows point to the allowed modes, paired arrows representing double degeneracy. The frequency level structure corresponds to that known for the energy levels of the corresponding molecules in chemistry.

through the foam below the crystal surface to permit coupling to defect modes. In Fig. 3(a)–3(e) the defect count goes from 1 to 6. Remarkably, the electromagnetic spectrum of each defect array geometry is isomorphous to the electronic energy levels of an analogous chemical molecule. For example, the defect array geometries correspond to a diatomic molecule, a triangular cyclopropenyl ion, up to benzene, six defects in a ring. Arrows in Fig. 3 point to the electromagnetic defect modes; paired arrows represent doubly degenerate frequencies associated with the defect array symmetry. For the case of six defects in a ring, the six electromagnetic frequencies are grouped in degeneracies of 1:2:2:1 as can be found for benzene energy levels in most elementary [23] chemistry books.

To reduce further the frequency of the evolving impurity band, and to satisfy better the condition $a \ll \lambda$, the gaps in the wires may be filled by high ε ceramic pellets or by inductive loading of the wires as suggested by Pendry *et al.* [22]. We believe that the effective medium limit $a \ll \lambda$ of a 3D wire mesh photonic crystal is of both physical and practical interest. Having light weight, and easily modified properties, they are likely to play a more important role in microwave and millimeter wave technology. Those possible applications include antenna structures, passive filter "windows," or frequency selective radomes, quasioptical amplifying structures, and stealthy surfaces.

This work was supported by Army Research Office Grant No. DAAH04-93-G-0227 and National Science Foundation Grant No. ECS-9310681.

[1] See, for example, the articles in the special issue of J. Opt. Soc. Am. B **10**, (1993).
[2] K. M. Ho, C. T. Chan, and C. M. Soukoulis, Phys. Rev. Lett. **65**, 3152 (1990).
[3] E. Yablonovitch, T. J. Gmitter, and K. M. Leung, Phys. Rev. Lett. **67**, 2295 (1991).
[4] H. S. Sozuer, J. W. Haus, and R. Inguva, Phys. Rev. B **45**, 13 962 (1992).
[5] S. Fan, P. R. Villeneuve, R. D. Meade, and J. D. Joannopoulos, Appl. Phys. Lett. **65**, 1466 (1994).
[6] E. Yablonovitch, Phys. Rev. Lett. **58**, 2059 (1987).
[7] S. John, Phys. Rev. Lett. **58**, 2486 (1987).
[8] E. Yablonovitch, T. J. Gmitter, R. D. Meade, A. M. Rappe, K. D. Brommer, and J. D. Joannopoulos, Phys. Rev. Lett. **67**, 3380 (1991).
[9] D. R. Smith, S. Schultz, N. Kroll, M. M. Sigalas, K. M. Ho, and C. M. Soukoulis, Appl. Phys. Lett. **65**, 645 (1994).
[10] T. Suzuki and P. K. L. Yu, J. Opt. Soc. Am. B **12**, 583 (1995).
[11] A. R. McGurn and A. A. Maradudin, Phys. Rev. B **48**, 17 576 (1993).
[12] M. M. Sigalas, C. T. Chan, K. M. Ho, and C. M. Soukoulis, Phys. Rev. B **52**, 11 744 (1995).
[13] J. P. Montgomery, IEEE Trans. Antennas Propag. **23**, 70 (1975).
[14] C. H. Tsao and R. Mittra, IEEE Trans. Antennas Propag. **32**, 478 (1984).
[15] G. Zarrillo and K. Aguiar, IEEE Trans. Antennas Propag. **35**, 1406 (1987).
[16] S. Singh and D. R. Wilton, IEEE Trans. Antennas Propag. **39**, 190 (1991).
[17] S. Kirkpatrick, Phys. Rev. Lett. **27**, 1722 (1971).
[18] C. Vassallo, J. Appl. Phys. **43**, 892 (1972).
[19] G. Diener and F. Kaseberg, Int. J. Solids Struct. **12**, 173 (1976).
[20] C. G. Granqvist and O. Hunderi, Phys. Rev. B **18**, 2897 (1978).
[21] H. G. Craighead, R. A. Burhman, and A. J. Sievers, Thin Solid Films **54**, 171 (1978).
[22] J. B. Pendry *et al.* (to be published).
[23] *Basic Principles of Chemistry*, edited by H. B. Gray and G. P. Haight, Jr. (W. A. Benjamin, New York, 1967), p. 317.